

Dynamics of temporal OCT4 regulation in human embryonic stem cells

L E Wadkin^{1*}, S Orozco-Fuentes¹, I Neganova², M Lako³, N G Parker¹, and A Shukurov¹

¹School of Mathematics, Statistics and Physics, Newcastle University, UK, NE17RU

²Institute of Cytology, RAS St Petersburg, Russia

³Bioscience Institute, Newcastle University, UK, NE17RU

*Correspondence: l.e.wadkin@ncl.ac.uk

Note: Work in progress, expected submission May 2020

ABSTRACT Pluripotency is the defining characteristic of human embryonic stem cells (hESCs), allowing them to differentiate into any somatic cell in the human body. For the promising clinical applications of hESCs, improved regulation of pluripotency and differentiation trajectories of *in-vitro* colonies is required. It has been shown that the pluripotency transcription factor OCT4 is inherited asymmetrically and that OCT4 is more similar in closely related cells. Here we use available experimental data to quantify the temporal dynamics of OCT4 over a cell lifetime. We evaluate the internal self-regulation of OCT4, quantify the intra-cellular fluctuations and consider the diffusive nature of OCT4 over time for individual and pairs of related cells. This quantitative framework provides a basis for comparison to other experiments, and the development of mathematical models of pluripotency.

SIGNIFICANCE 120 words

INTRODUCTION

Human embryonic stem cells (hESCs) form colonies through repeated mitosis and have the ability to differentiate into all somatic cell types in the human body: the *pluripotency* property. The pluripotency of hESCs is their defining characteristic, making them essential for developments in drug discovery, regenerative and personalised medicine (1–6). These promising clinical applications of hESCs require great control over colony pluripotency, homogeneity and differentiation trajectories *in-vitro* (7), yet this remains challenging.

The control and optimisation of pluripotency across colonies is difficult due to the complex inter-regulatory dynamics of pluripotency. At the single-cell level, pluripotency is inherently stochastic. It has been suggested that pluripotency is not well defined at the single-cell level but is instead a statistical property of a cell population (8, 9). Cell pluripotency is also affected by many factors: the local environment (10, 11), interactions with neighbours (12, 13), the cell cycle (14) and the substrate (15). On the colony scale, complex collective effects of pluripotency can be seen. Differentiation is spatially disordered, with bands of differentiated cells occurring around colony edges (13, 16).

Pluripotency maintenance relies on the inter-regulation of pluripotency transcription factors (PTFs): the genes OCT4, SOX2 and NANOG (17–19). The fluctuations of PTFs cause

variation in pluripotency in different sub-populations (17). The differentiation of a stem cell into a specialised cell is the departure from the pluripotent state led by PTF destabilisation and their interaction with chemical signalling pathways (17, 20, 21). This decision of a stem cell to either remain pluripotent or to differentiate is known as its fate decision. It is unknown how much cell fate decisions are led by inherited factors versus environmental factors and intracellular signalling as even clonal (genetically identical) cells under the same conditions make different fate decisions (22). Colonies exhibit heterogeneous sub-populations of cells with differing levels of PTF expression (17, 20, 23) which suggests a play-off between disruptive single-cell and regulatory community effects (8, 9, 13, 16).

On the intra-cellular level, it has been shown that a narrow range of PTF abundance is necessary for maintained pluripotency (24, 25) and that small fluctuations bias cell fate decisions in the G1 phase of the cell cycle (26). Furthermore, the PTFs are inherited asymmetrically as a cell divides, biasing the fate of the daughter cells and contributing to colony heterogeneity (27–29) with the decision to differentiate largely determined before any differentiation stimulus is added (27). As PTF fluctuations are inherently stochastic (8, 9, 30), it is important to quantify their temporal dynamics and the knock-on effects to cell fate. In this paper we build upon the previously

published work of Ref. (27) which considers OCT4 intensity levels and provides experimental data with rich opportunities for further quantitative analysis and mathematical modelling.

Mathematical models are a powerful tool through which to deepen our understanding of the inherent, systematic behaviours of stem cells (31). Many current models focus on describing pluripotency and cell fate decisions to guide the optimisation and control of pluripotency in the laboratory (32) and are informed by recent studies of fluctuations of PTFs throughout colonies (9, 26, 27) and the spatial patterning of differentiation (13, 16). Many models use complex coupled stochastic differential equations to describe PTF fluctuations (33–35) while others use a gene network analysis framework (36, 37) or take a mechanistic approach (38).

Although the dynamics of OCT4 are complex, affected by many genetic factors and closely regulated by the other PTFs (17, 21, 39), here we aim to isolate autonomous properties of OCT4 to facilitate the development of descriptive mathematical models. This quantification of OCT4 will provide a basis for identifying systematic similarities and differences between PTFs in future experiments. As our quantitative understanding of PTF regulation increases, more complex regulatory properties can be considered to build fundamental models.

Here we use the experimental data from Ref. (27) of OCT4 levels in cells in a growing hESC colony to quantify the dynamics of intra-cellular OCT4. In addition to the OCT4 splitting dynamics and fluctuations described in Ref. (27), we describe quantitatively the fluctuations in OCT4 in relation to cell fate and the addition of the differentiation agent BMP4. We quantify the self-regulation of OCT4 through anti-persistence and characterise it within the diffusion framework. This quantitative analysis, along with Ref. (27), provides the basis for developments in mathematical and statistical models of pluripotency.

MATERIALS AND METHODS

Experiment

The experiment considered here was carried out by Purvis Lab (University of North Carolina, School of Medicine), and published in Ref. (27). The OCT4 levels (mean OCT4-mCherry fluorescence intensity) in a human embryonic stem cell (H9) colony were determined by antibody staining (mouse anti-OCT4 antibody MABD76, EMD Millipore) and cells were live-imaged for approximately 70 hours. At 40 hours the differentiation agent BMP4 was added to the cells. The cell IDs, ancestries and positions were extracted along with their OCT4 immuno-fluorescence intensity values (reported in arbitrary fluorescence units a.f.u.). Each cell was classified according to its final fate status as either pluripotent, differentiated or unknown using expression levels of CDX2. Full experimental details are given in Ref. (27). This illuminating study by S. C. Wolff et. al., provides rich opportunities for further quantitative analysis.

Colony growth summary

Here we give an introduction to the colony dataset. The colony begins from 30 cells and grows over 68 hours (817 timeframes) to 381 cells, with 1274 cell cycles considered within this time. A differentiation agent BMP4 was added to the cells at 40 hours. In Ref. (27) the cells are categorised according to their final cell fate status as pluripotent (518 cells), differentiated (133 cells) or unknown (623 cells).

For every cell in the colony there is a corresponding time series of the abundance of OCT4 within the cell during its lifetime: $OCT4(t_1)$, $OCT4(t_2)$, ..., $OCT4(t_n)$, where t_1 and t_n are the start and end of the cell cycle for the cell, respectively. We will use the notation t_i to describe time-steps in terms of the cell cycle and T_i for experimental time (between 0 and 68 hours).

Snapshots of the colony at times $T = 0$ h, $T = 20$ h, $T = 40$ h (the time BMP4 is added) and $T = 68$ h (the final recorded time) colour coded by OCT4 intensity are shown in Figure 1. There is clear spatial patterning of cell fates within the colony, with clustering of pluripotent cells in the centre and differentiated cells around the top edge of the colony. Spatial analysis shows that this patterning begins emerging at around $T = 20$ hours (20 hours before BMP4 addition) for differentiated cells, and at around $T = 50$ hours (10 hours post BMP4 addition) for pluripotent cells Ref. [Sirio]. Although here we focus on quantifying the temporal regulation in OCT4, we must keep in mind that there is a spatial correlation between the cell fates.

An analysis of the number of cells in the colony over time, $N(T)$, is given in the Supplementary Information (Figure S1). The whole colony follows exponential growth, with a doubling time of 16 ± 0.01 hours, as noted in Ref. (27). This doubling time is consistent with some reports (40, 41) but is significantly shorter than other estimates of 24 hours (42). The corresponding doubling times for the different cell fates are 17 ± 0.004 , 14 ± 0.01 and 16 ± 0.01 hours for pluripotent, differentiated and unknown cells respectively. As expected, the pluripotent cells proliferate significantly faster than the differentiated cells.

Dataset

The original dataset is available from Ref. (27), providing cell IDs, cell ancestries, cell positions, cell fates and mean OCT4-mCherry fluorescence intensities. Cell IDs in this manuscript are consistent with those in the original dataset.

Quantitative analysis

The quantitative analysis in both Ref. (27) and this manuscript were performed using MATLAB.

Averaging and errors

When average values are given the type of averaging (mean or median) is specified. For means the errors are given in the

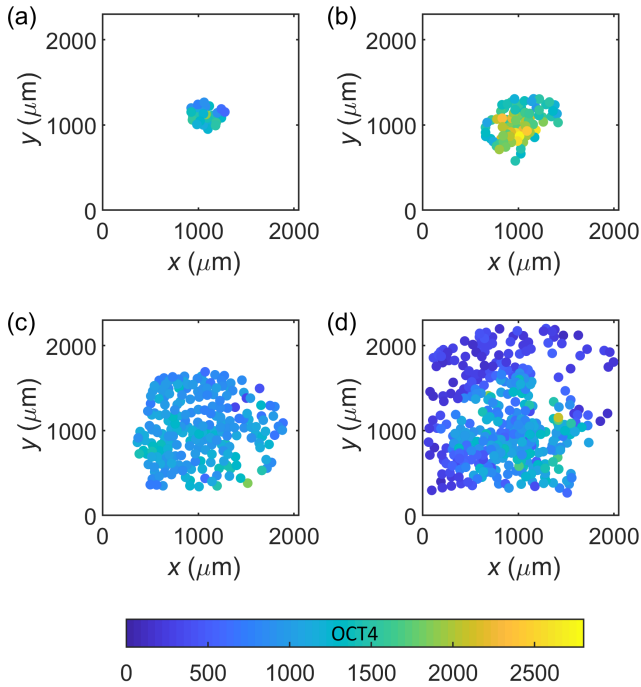


Figure 1: Snapshots of the colony at (a) $T = 0$ h, (b) $T = 20$ h, (c) $T = 40$ h (at the addition of BMP4) and (d) $T = 68$ h (final time). The cells are coloured according to their OCT4 intensity levels. Note that the circles are not indicative of cell or nucleus size.

form \pm standard deviation (standard error in the mean). For medians the errors represent the lower and upper quartiles or the interquartile range as specified.

Correlation coefficient

The correlation between two OCT4 time series is calculated using Person's correlation coefficient.

De-trending

We remove trends from the data when it is necessary to analyse fluctuations about any present trend. We used MATLAB's inbuilt function *detrend* which subtracts the best-fit line from the data.

Line fittings

Lines of best fit throughout were calculated using a least-squares method and the errors given represent the 95% confidence interval of the parameters.

Statistical testing

To test the null hypothesis that a distribution is Gaussian, we use both the one-sample Kolmogorov Smirnov and Shapiro-Wilk tests. To test the null hypothesis that two non-parametric distributions are from the same distribution we use the two-sample Kolmogorov Smirnov test.

The Laplace distribution

We consider the Laplace distribution, sometimes referred to as the double exponential distribution, using the notation $\text{Laplace}(\mu^\dagger, b)$ to distinguish from the usual parameter μ in $\text{Normal}(\mu, \sigma^2)$. The parameters can be estimated using the maximum likelihood estimators $\hat{\mu}^\dagger$ and \hat{b} , where $\hat{\mu}^\dagger$ is the sample median and \hat{b} is the mean absolute deviation from the median

$$\hat{b} = \frac{1}{N} \sum_{i=1}^N |x_i - \hat{\mu}^\dagger|.$$

This method of parameter estimation was used in the manuscript to find Laplace distributions to describe the change in OCT4 between time-steps.

The Hurst exponent

The Hurst exponent, H , is a measure of the long term memory, or the scale of the self-similarity properties of a time series. It is defined as

$$E \left[\frac{R(n)}{S(n)} \right] = Cn^H \text{ as } n \rightarrow \infty,$$

with $R(n)$ the range of the first n cumulative deviations from the mean and $S(n)$ their standard deviation. $E[\cdot]$ denotes the expected value, n is the number of data points in the time series and C is a constant.

The quantity R/S is known as the rescaled range and measures how the apparent variability changes with the length of time considered. For a time series X_1, X_2, \dots, X_n , with mean $m = \frac{1}{n} \sum_{i=1}^n X_i$, R_t can be calculated as

$$R_t = \max(Z_1, Z_2, \dots, Z_t) - \min(Z_1, Z_2, \dots, Z_t),$$

where

$$Z_t = \sum_{i=1}^t X_i - m \text{ for } t = 1, 2, \dots, n.$$

Further details on the Hurst exponent, other methods of estimation and its relation to fractional Brownian motion can be found in Refs. (43–46).

Autocorrelation analysis

Autocorrelations were calculated using MATLAB's *autocorr* function (Econometrics Toolbox). The autocorrelation C_i of a time series between x_t and x_{t+i} for time-lag i is given as

$$C_i = \frac{1}{T\sigma} \sum_{t=1}^{T-i} (x_t - \bar{x})(x_{t+k} - \bar{x}),$$

where σ is the sample variance of the time series. The correlation time is defined as $\tau = \int_{-\infty}^{\infty} C(t)dt$. The auto-correlations can be described by the function $C = \cos(2\pi t/a)e^{-t/b}$ (47).

Random walk theory

We apply the theory of random walks to the OCT4 time

series to test if the OCT4 intensity drifts diffusively. Traditionally used for the migration of particles, the mean square displacement (MSD, mean square difference or mean square fluctuation) is calculated as $\text{MSD} = \langle |x(t) - x(0)|^2 \rangle$, where $x(t)$ and $x(0)$ are the current (at time t) and starting positions, and $\langle \rangle$ denotes an average over all particles. If the motion is diffusive (Brownian) then the MSD increases linearly with time in the manner $\text{MSD} = 2Dt$. Sub-diffusion is shown by $\text{MSD} \propto t^\alpha$ with $\alpha < 1$ and super-diffusion with $\alpha > 1$. Here we consider the one dimensional version, the mean square difference. For further information on the use of random walks in mathematical biology see Refs. (48, 49).

RESULTS

For every cell in the colony there is a corresponding time series of the abundance of OCT4 within the cell during its lifetime: $\text{OCT4}(t_1), \text{OCT4}(t_2), \dots, \text{OCT4}(t_n)$, where t_1 and t_n are the start and end of the cell cycle for the cell, respectively. The time frames are five minutes.

The analysis in Ref. (27) shows that upon cell division the ratio between the OCT4 values of sister cells is centred around a 1:1 distribution, meaning that although asymmetric pluripotency splitting is seen (for example, 38% of divisions occur in the ratio 5:6 or more extreme), on average sister cells start with similar levels of OCT4. It is also shown that OCT4 levels are more similar in closely related cells, i.e., sister cells and cousins cells show significant similarity when compared with random pairs of cells. Here we will quantify how this drift in OCT4 similarity between related cells occurs over cell lifetimes.

OCT4 in sister cells

We can consider the strength of the correlation in temporal OCT4 in sister cells over their whole lifetimes by calculating the correlation coefficient, ρ . Before calculating the correlation, each OCT4 time series was de-trended to account for any confounding similarities in sister cells that may be present due to their shared environment. The distribution of ρ for all sister cells, those of the same fates, and those before and after BMP4 addition are shown in Figure 2a and 2b. The mean correlation for all sister cells is $\bar{\rho} = 0.5 \pm 0.3(0.01)$, a significant positive correlation. This is consistent between sister cells of the same fate, with $\bar{\rho} = 0.5$ for pluripotent ($\pm 0.3(0.02)$), differentiated ($\pm 0.2(0.04)$) and unknown cells ($\pm 0.3(0.02)$). The Kolmogorov Smirnov test provides no evidence at the 95% confidence level to reject the null hypothesis that the distributions are the same. Sister cells before BMP4 addition show a slightly less strong correlation, with $\bar{\rho} = 0.3 \pm 0.2(0.03)$, compared to those after BMP4 addition, with $\bar{\rho} = 0.5 \pm 0.3(0.01)$. The Kolmogorov Smirnov test provides evidence at the 95% level to reject the null hypothesis that the two distributions are the same. These results quantify

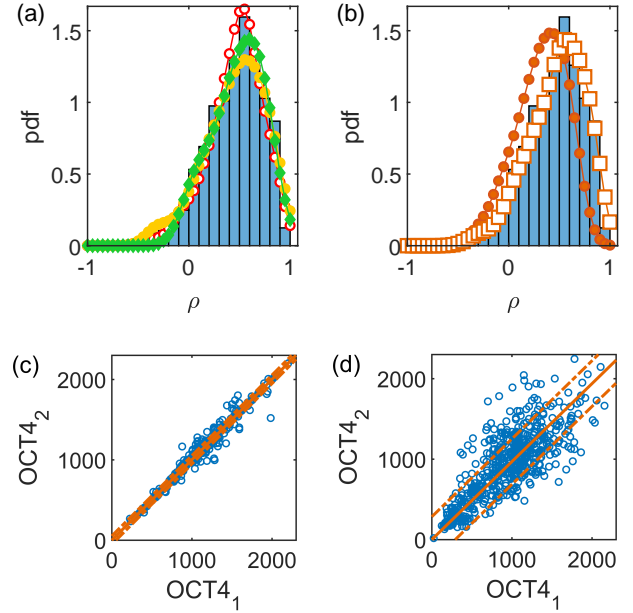


Figure 2: The correlation, ρ , between temporal OCT4 in sister cells. In both panels the blue solid histogram shows the distribution of ρ for all sister cells with additional distributions for cases where both sisters cells were (○) pluripotent (red unfilled circles), differentiated (green diamonds) and unknown (yellow filled circles) and (○) before (filled circles) and after (unfilled squares) BMP4 addition. OCT4 values for all sister pairs (○) at the start and (○) end of their cell cycles. Lines of best fit (orange solid lines) with standard errors in predicting a future observation (dashed lines) of (○) $\text{OCT}_1 = (1 \pm 0.003)\text{OCT}_2$ with $R^2 = 0.98$ and (○) $\text{OCT}_1 = (0.97 \pm 0.02)\text{OCT}_2$ with $R^2 = 0.78$.

the regulation between closely related cells and further illustrate that this regulation is systematic and importantly, still present when confounding external trends are removed.

We can also quantify how this correlation between sister cells drifts throughout their lifetimes. The initial and final OCT4 values for all sister cells are shown in Figure 2c and 2d. The initial values follow a very close relationship (as also shown by the OCT4 ratio splitting distribution in Ref. (27)), with a correlation of $\rho = 0.99$ and the trend line $\text{OCT}_1 = (1 \pm 0.003)\text{OCT}_2$. (Note that the labelling of cell 1 and cell 2 is entirely arbitrary.) By the end of their respective lifetimes, the distribution spreads, with a correlation of $\rho = 0.78$ and a line of best fit $\text{OCT}_1 = (0.97 \pm 0.2)\text{OCT}_2$.

In the next section we will consider the behaviour of OCT4 from the initial point of possible asymmetric inheritance, to the final time before mitosis at the end of the cell lifetime, to characterise how this drift of similarity in sister cells occurs.

Temporal OCT4 dynamics

In this section quantify the temporal behaviour of OCT4 dynamics on the cellular level over the course of a cell lifetime. We consider the variability between discrete time-steps and quantify the self-regulatory behaviour of OCT4 using several methods.

Variability between timesteps

It has been shown that even small fluctuations in PTF abundance impact cell fate (26) with both high and low PTF values resulting in differentiation (24, 25). Mathematical models of PTF fluctuation will allow for the description of pluripotency over discrete time-steps, fitting for time-lapse experiments such as the one considered here (27). It is therefore necessary to quantify these integral fluctuations. First, we will consider the change in the intra-cellular OCT4 abundance between the five minute time intervals, t_1, t_2, \dots, t_n , as $\Delta\text{OCT4} = \text{OCT4}(t_i) - \text{OCT4}(t_{i-1})$. It is likely that a large proportion of these individual fluctuations will be due to experimental noise, but considering all of these values together reveals the average behaviour.

The distribution of ΔOCT4 for cells of different fates (pluripotent, differentiated and unknown) before and after BMP4 addition is shown in Figure 3a and 3b. Pre-BMP4, the change in OCT4 is centred around zero (although the individual values range from -1300 to 1200) with standard deviations of 82, 72 and 68 for the pluripotent, differentiated and unknown groups, respectively. This means that, on average, the change in OCT4 is isotropic for cells of all fates. There is no preference for the abundance to increase or decrease in a time-step, the fluctuations are symmetric overall. Interestingly, although symmetric, the distributions are not Gaussian (confirmed by the Kolmogorov-Smirnov and Shapiro-Wilk tests at the 95% confidence level) due to a narrower and steeper peak, shown in Figure 3c for pluripotent cells. A Laplace distribution, $\text{Laplace}(\mu^\dagger, b)$, better fits the experimental data in all cases, see Figure 3c for pluripotent cells, with the parameters $\mu^\dagger = -1.3$ and $b = 46.9$. The distributions and fittings for differentiated and unknown cells are given in the Supplementary Information, Figure S2.

Post-BMP4 addition, the distributions for all cell fates become significantly narrower, with standard deviations of 72, 43 and 52 for pluripotent, differentiated and unknown cells respectively, as seen in Figure 3b. This reduction in variance, although apparent across all cell fates, is most pronounced for differentiated cells with a 40% reduction in the standard deviation (with a 12% reduction for pluripotent cells and 25% for unknown cells). There is also a subtle skew in the differentiated and unknown cells towards negative values of ΔOCT4 which is consistent with the fact that the OCT4 levels overall decrease after the BMP4 addition. The narrowing of the distributions show a preference to smaller changes in OCT4 in all cell fates provoked by the differentiation agent. This could be driven by induced selectivity caused by the

BMP4 addition (i.e., the BMP4 causes a systematic change, preferring smaller ΔOCT4 values), or it could suggest some collective self-regulation (8). Further experiments are needed to investigate if this is a collective behaviour effect, considering the effect of colony size. It is expected, since the differentiated cells are most affected by the BMP4, that this group show the biggest reduction in variation and therefore the strongest regulation in their OCT4 values. Again, the distributions can be described by a Laplace distribution, with the parameters $\mu^\dagger = 0.0$ and $b = 34.3$ for pluripotent cells, shown in Figure 3d. The distributions and fittings for differentiated and unknown cells are given in the Supplementary Information, Figure S2.

This information quantifies step changes in OCT4 for mathematical models, suggesting the use of the Laplace distribution to simulate variation and shows that the addition of BMP4 provokes tighter self-regulation across all cell fates. It also highlights that even between small time increments such as these, the fluctuations post BMP4 should be considered separately for cells of different fates, not only in terms of their average, as expected, but also their variability. Note that this allows us to capture the nature of the variation in OCT4 only and further aspects of the behaviour need to be considered to fully describe the OCT4 regulation over time.

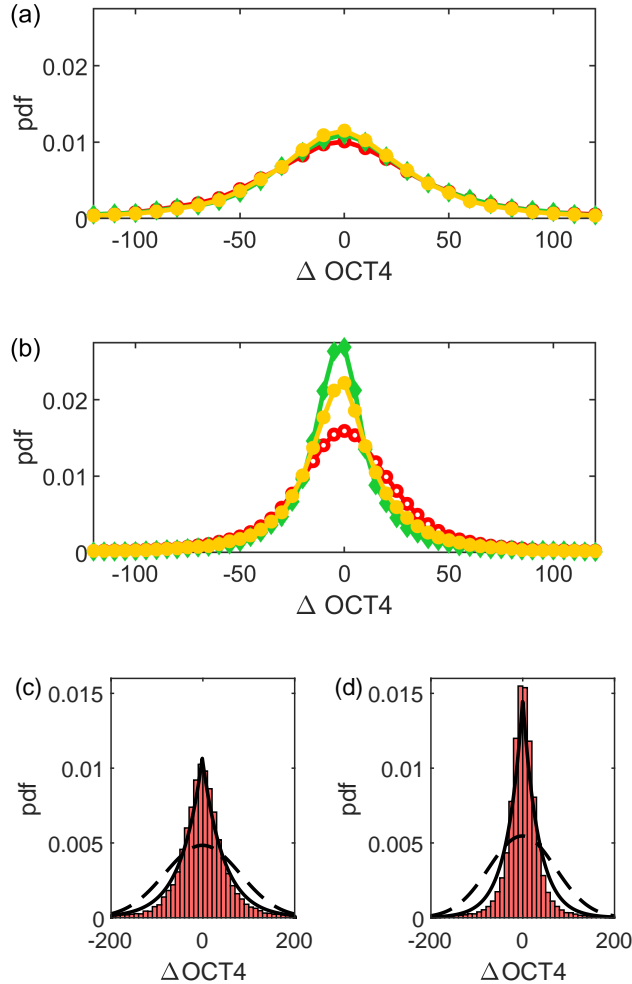


Figure 3: Distributions of the change in OCT4 between the five minute time frames (ΔOCT4) for pluripotent (red open circles), unknown (yellow filled circles) and differentiated cells (green filled diamonds) for (a) before and (b) after BMP4 is added. The distribution of ΔOCT4 for pluripotent cells (c) before and (d) after BMP4 addition. Solid lines show the Laplace distribution fittings, $\text{Laplace}(\mu^\dagger, b)$, with the parameters $\mu^\dagger = -1.3$ and $b = 46.9$ pre-BMP4, and $\mu^\dagger = 0.0$ and $b = 34.3$ post-BMP4. Dashed lines show the Normal distribution fittings.

OCT4 self-regulation

To investigate the self-regulation and internal memory of OCT4 during a cell cycle, we consider three related approaches, the Hurst exponent, the autocorrelation function and diffusion analysis.

The Hurst exponent, $0 < H < 1$ is a measure of the long term memory of a time series. If a series is Brownian, $H = 0.5$, then the fluctuations are isotropically random, with the variable just as likely to increase as decrease at each time-step. If the series is persistent, $H > 0.5$, then at each time-step the series is more likely to fluctuate in the same direction as the previous step, i.e., if in the last time-step there was an increase, it is more likely there will be another increase during the next time-step. For anti-persistence, $H < 0.5$, the series is less likely to fluctuate in the same direction as the previous step.

The Hurst exponent was calculated for all cells which live longer than 50 time frames (4.16 hours). The distribution of all H values for those cells is shown in Figure 4a, with H split by cell fate in Figure 4b. Considering all fates together, the mean value of H , \bar{H} , is 0.38 ± 0.09 (0.003), showing significant anti-persistence. This shows the self-regulation of OCT4 on the intra-cellular scale, if the OCT4 value has just increased, it is more likely to next decrease, and vice versa. This is the case across each cell fate group, with means of $\bar{H} = 0.37 \pm 0.09$ (0.004), 0.40 ± 0.09 (0.008) and 0.39 ± 0.09 (0.004) for pluripotent, differentiated and unknown cells, respectively. Although the means are within errors of one another, the Kolmogorov Smirnov tests reject the null hypothesis that the pluripotent and differentiated H distributions are the same at the 95% level. There is no significant difference in H before and after the BMP4 addition (confirmed by the Kolmogorov Smirnov test at the 95% level and shown in the Supplementary Information, Figure S3) suggesting this aspect of the self-regulatory behaviour is inherent within the cells and unchanged by the differentiation stimulus. This quantification via the Hurst exponent is directly transferable to use in fractional Brownian motion modelling methods (43–46).

The anti-persistence can be further explored by considering the autocorrelation of the time series. The autocorrelation is the correlation of a time series with itself at increasing time lags, hence $-1 \leq C \leq 1$ where $C = 0$ signifies no correlation, $C < 0$ a negative correlation (corresponding to anti-persistence) and $C > 0$ a positive correlation (persistence). The decay of the autocorrelation to zero (scaled to cell lifetimes) is presented in the Appendix in Ref.(27) and here we extend this to quantify the periods of anti-persistence and consider the periodic nature of the autocorrelation.

Typical autocorrelations for example cells are shown in Figure 5. The majority of the cells follow an autocorrelation similar to the one shown in Figure 5a (Cell ID 46), with

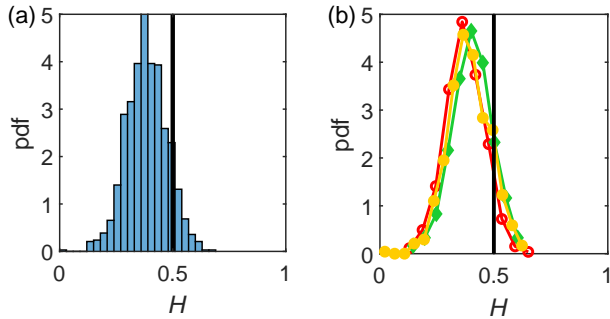


Figure 4: The Hurst exponent, H for (a) all cells and (b) all pluripotent (red), unknown (yellow) and differentiated (green) cells. The black lines show $H = 0.5$, the value for Brownian fluctuations.

initial persistence declining to zero, followed by a period of anti-persistence before the autocorrelation settles at zero. There are, however, other behaviours evident. Some cells show several periods of anti-persistence, as in Figure 5b (Cell ID 14), with others showing a final period of persistence before settling at zero, as in Figure 5c (Cell ID 43). The corresponding time series of OCT4 for each example cell are shown in Figure 5d-f. The periods of persistence are visible as trends in OCT4 (either continued increase or decline), with anti-persistence visible as fluctuations about a horizontal line.

Anti-persistence of at least one hour duration is seen in 99% (1255/1274) of cells, and for at least five hours in 86% (1090/1274) of cells. Of the cells with at least one hour anti-persistence visible, 78% show one period of anti-persistence (as in Figure 5a), 18% two periods (as in Figure 5b), and the remaining 4% three or more. The first time anti-persistence occurs, t_{AP} , can be extracted for each individual cell. The distribution of t_{AP} for cells with at least one hour anti-persistence is shown in Figure S4 and reveals the critical cell cycle time in which it first occurs. In all cells with anti-persistence, it has begun by 8 hours into the cell cycle (just over half a cell cycle (27)), suggesting that before they reach the latter halves of their lifetimes the internal self-regulation of OCT4 begins. This could be due to the memory effects or the down-regulation of the PTF which occurs prior to mitosis (50, 51).

The periodic nature and decay of the autocorrelation can be captured by the function $C = \cos(2\pi t/a)e^{-t/b}$ (47) (note that this periodicity in the autocorrelation does not necessarily imply periodicity in the time series). These fittings are shown in the Supplementary Information, Figure S5, for 25 random cells in the colony. This quantifies the temporal, periodic decay in the autocorrelation, with the parameter a representing the time-scale of the periodicity, and b the time-scale of the decay (the correlation decay time). Histograms of a and b for all 1274 cells are shown in Figure 6. Both distributions are skewed, with medians of 11.7 h and 3.0 h, and 90th percentiles of 30 h and

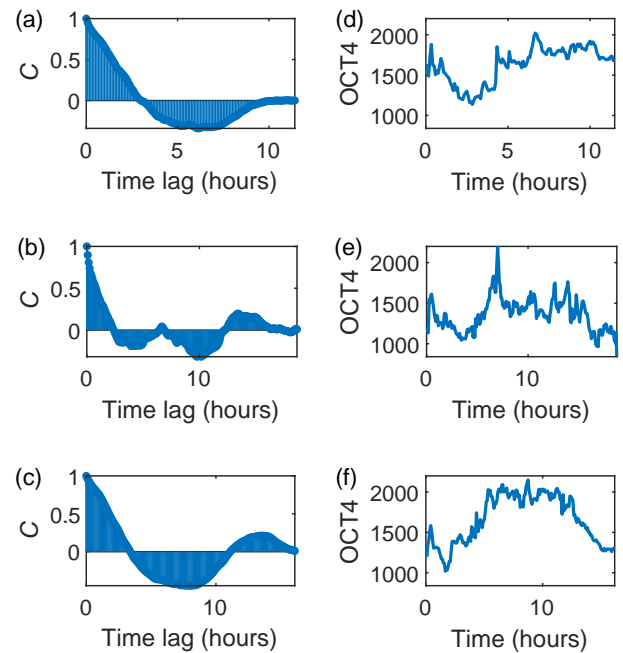


Figure 5: Typical autocorrelations showing (a) a period of anti-persistence before settling at zero correlation, (b) two periods of anti-persistence followed by persistence and (c) a period of anti-persistence followed by a period of persistence. The panels (d)-(f) show the OCT4 variation in time for these cells respectively. The average behaviour is similar to that in (a).

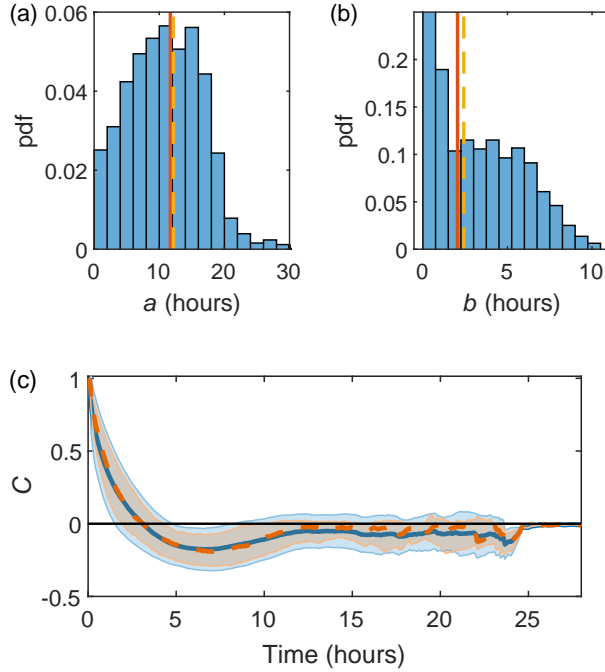


Figure 6: The distributions of the parameters (a) a and (b) b from all $C = \cos(2\pi t/a)e^{-t/b}$ autocorrelation fittings. The parameter estimates using the mean and median autocorrelations for all cells are $a = 11.7 \pm 0.92$ and 12.16 ± 0.69 and $b = 2.05 \pm 0.23$ and 2.42 ± 0.21 and are shown as a red solid and yellow dashed line, respectively. (c) The mean (blue solid with standard deviation error bars) and median (orange dashed, with interquartile range error bars) autocorrelation for all cells with increasing time lag.

7 h for a and b respectively. This quantifies the characteristic time-scale of the periodicity and the correlation decay time as less than 7 hours in 90% of cases. The correlation time is defined as $\tau = \int_{-\infty}^{\infty} C(t)dt$, with a mean correlation time across all cells of $\bar{\tau} \approx 0 \pm 0.002$ h. The distribution of all correlation times is shown in the Supplementary Information, Figure S4.

We can identify the average behaviour by considering all autocorrelations for all cells. The mean (and standard deviation) and median (and interquartile range) autocorrelations \bar{C} for all cells is shown in Figure 6c. Notably the mean and median are comfortably within errors of each other and the autocorrelation is robust to the chosen averaging method. The average autocorrelation decreases to zero at around three hours, followed by a period of negative autocorrelations indicative of anti-persistent behaviour between approximately three and 12 hours. By 13 hours, the average autocorrelation settles at zero, showing no internal memory past this time. These observations are robust to cell fate and the equivalent autocorrelations for pluripotent, differentiated and unknown cells are shown in the Supplementary Information, Figure S6.

This shows that during a cell cycle, there is long-term memory in the abundance of OCT4 up to around 12 hours, but the nature of the effect differs over this time with initial persistence being replaced by anti-persistence. Notably, the mean autocorrelation is not fully described by $\cos(2\pi t/a)e^{-t/b}$, as the full scale of the anti-persistence is not captured, shown in the Supplementary Information, Figure S6.

A further method of quantifying the internal regulation of OCT4 is to consider the diffusive behaviour of the time series. The theory of diffusivity and random walks is widely used across many biological applications, including stem cells and so it is important to quantify the OCT4 behaviour within this framework (48, 49, 52–55).

Each cell has an initial OCT4 value at the start of its lifetime, denoted OCT_0 . Here we will consider this to be the OCT4 value half an hour after cell division to allow for the asymmetric division of OCT4. The mean square difference of OCT4 over time, $MSD(t)$, can be calculated as $\langle |OCT4(t) - OCT4_0|^2 \rangle$, where $\langle \rangle$ denotes the average across all 1274 cells. The MSD for all cells over all times is shown in the Supplementary Information, Figure S7. Looking specifically at early times, Figure 7a, the distinct sub-diffusive behaviour of the MSD is visible, with $MSD \propto t^\alpha$, $\alpha = 0.8 < 1$. When split by cell fate as shown in Figure 7b, the MSD shows similar sub-diffusive behaviour in each fate group with $\alpha = 0.6$ for pluripotent and $\alpha = 0.7$ for both differentiated and unknown cells. Considering the cells before and after BMP4 addition separately reveals stronger sub-diffusive behaviour after BMP4 treatment, Figure 7c.

This sub-diffusivity is consistent with the anti-persistence illustrated by the Hurst exponent and autocorrelation. The MSD for all cells is well described by $MSD = \beta t^\alpha$ for the first 15 hours in the cell cycle, with $\beta = 24000 \pm 1000$, $\alpha = 0.8 \pm 0.02$ and $R^2 = 0.99$. Post 15 hours, the MSD deviates from this fit, shown in Figure S7. This could be due to less cells being considered in this time (as many divide before 15 hours) or a systematic effect due to the cells approaching the M phase. The MSD for cells of different fates can be described by $MSD = \beta t^\alpha$, with $\beta = 24000 \pm 1000$, $\alpha = 0.8 \pm 0.02$ ($R^2 = 0.99$) for pluripotent cells, $\beta = 21000 \pm 1300$, $\alpha = 0.7 \pm 0.04$ ($R^2 = 0.97$) for differentiated cells and $\beta = 26000 \pm 700$, $\alpha = 0.7 \pm 0.01$ ($R^2 = 0.99$) for unknown cells, shown in Figure 7b. The MSD for cells before and after BMP4 has the parameters $\beta = 42000 \pm 1500$, $\alpha = 0.5 \pm 0.02$ ($R^2 = 0.97$) up to the first 10 hours, and $\beta = 23000 \pm 800$, $\alpha = 0.8 \pm 0.02$ ($R^2 = 0.99$) for the first 12 hours, respectively, shown in Figure 7c. The fits are shown for all times in the Supplementary Information, Figure S7 and S8.

For mathematical modelling purposes, this drift in OCT4 values can be considered between sister cells with the diffusion framework. We have shown that, on average, the intracellular OCT4 abundance behaves in a sub-diffusive manner throughout a cell lifetime. This has a knock-on effect for the relationship between sister cell OCT4 which is presented in the Supplementary Information (Figure S9-11).

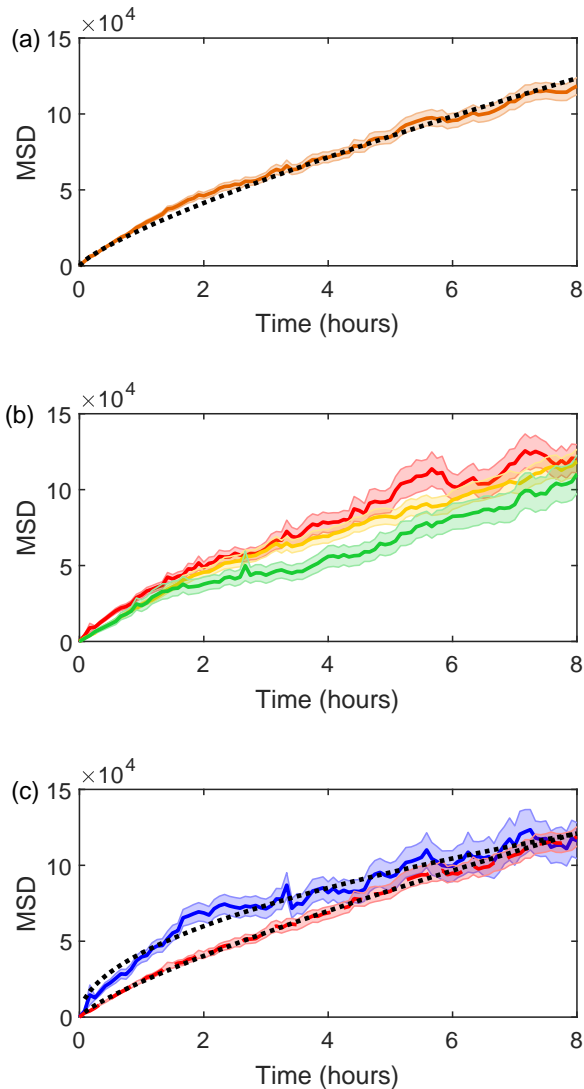


Figure 7: The MSD between 0 and 8 hours with standard error bars and the fits $\text{MSD} = \beta t^\alpha$ (black dotted lines) for (a) all cells, $\beta = 24000 \pm 1000$, $\alpha = 0.8 \pm 0.02$ ($R^2 = 0.99$), (b) pluripotent (red), $\beta = 36000 \pm 1700$, $\alpha = 0.6 \pm 0.02$ ($R^2 = 0.99$), differentiated (green), $\beta = 21000 \pm 1300$, $\alpha = 0.7 \pm 0.04$ ($R^2 = 0.97$) and unknown (yellow), $\beta = 26000 \pm 700$, $\alpha = 0.7 \pm 0.01$ ($R^2 = 0.99$) cells and (c) cells before (blue solid line), $\beta = 42000 \pm 1500$, $\alpha = 0.5 \pm 0.02$ ($R^2 = 0.97$) and after (red dashed line) BMP4 addition, $\beta = 23000 \pm 800$, $\alpha = 0.8 \pm 0.02$ ($R^2 = 0.99$).

This further quantifies the self-regulatory behaviour of OCT4 within the diffusion framework, a fundamental starting point for many mathematical models. The anti-persistence of OCT4 suggests possibilities for mathematical modelling methods to capture the internal regulation of pluripotency, including fractional Brownian motion and correlated random walk theory.

DISCUSSION

Promising clinical applications of hESCs require tight control over the pluripotency of *in-vitro* colonies. It has been shown that even small PTF fluctuations can bias cell fate decisions and that PTFs are inherited asymmetrically upon cell division (26–29). It is therefore necessary to quantify the dynamics of key PTFs to further our understanding of how pluripotency is regulated and assist in the development of mathematical modelling. Rigorous quantification also provides the basis for experimental comparisons, and the identification of systematic and universal behaviours. Here we have used a published data set from Ref. (27) to analyse and quantify the dynamics of the pluripotency transcription factor OCT4.

The colony considered grows exponentially, with changing proportions of pluripotent, differentiated and unknown cells. Snapshots of the colony show some spatial patterning of the OCT4 abundance (Figure 1), with higher OCT4 abundant cells clustered in the colony centre. A spatial analysis of the colony can be found in Ref. [Sirio]. Here we have focused on the quantification of the temporal dynamics of OCT4.

Time-lapse experiments such as the one considered here provide a wealth of opportunities for the quantification of temporal PTF regulation which can be compared to, and enhance, current biological knowledge. For example, a sharp decline in OCT4 levels occurring before cell division is noted in Ref. (27), in keeping with the transcription factor down regulation known to occur before mitosis (50, 51). This phenomena can be quantified, with the decrease in OCT4 beginning, on average, 35 minutes (0.58 hours) before cell division, lasting for 15 minutes (0.25 hours), and showing a reduction of 22%. This is shown for all cells before BMP4 addition in the Supplementary Information, Figure S12.

Ref. (27) reveals that sister cells show more closely related OCT4 values than pairs of random cells. Here we take this a step further by quantifying their temporal dynamics in relation to one another. Taking into account any common trends which may affect both cells due to their shared environment, the sister cells before BMP4 show a moderate correlation with each other with a correlation coefficient of 0.5. This is reduced to a slight correlation for pairs that exist after the BMP4 addition (0.3). The fact that these correlations still occur after detrending further highlights the inherent similarities between related cells. We then consider the OCT4 behaviour over cell lifetimes to explore the manner in which this drift in similarity occurs. The behaviour is summarised in the schematic in Figure 8.

Stochastic fluctuations in OCT4 have been shown to bias cell fate (26) with evidence of asymmetric noise leading to noise-mediated cell plasticity (30). Here we see the change in OCT4 between each 5 minute time interval is isotropic, with an average of zero. A natural assumption in model development would be to simulate this symmetric time-step change in OCT4 with a Normal distribution, however the distribution of all these changes best fits a Laplace distribution. Further experimental

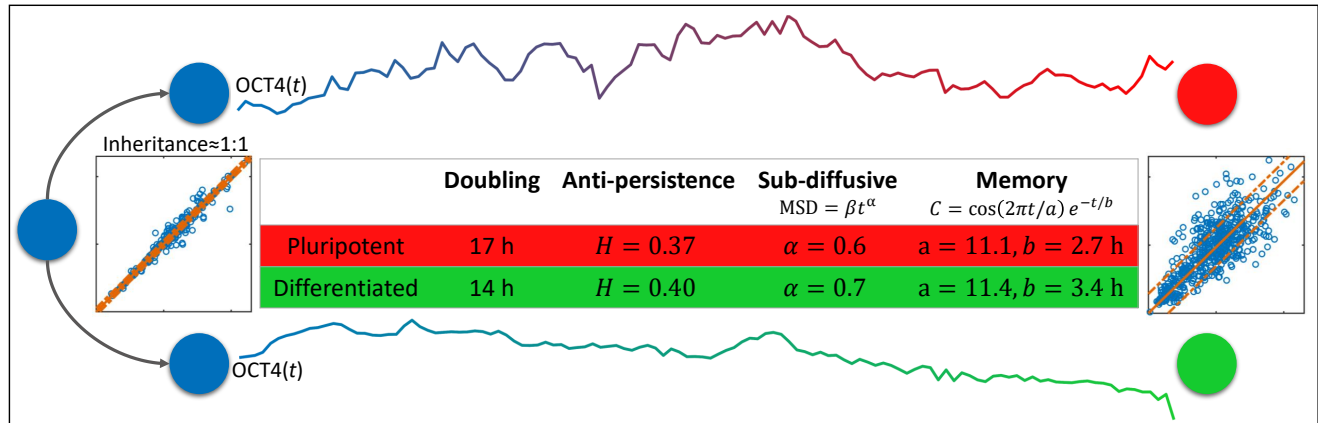


Figure 8: An illustration of the dynamics in OCT4 over a cell lifetime. OCT4 is split, possibly asymmetrically but on average in a 1:1 ratio (27), before fluctuating in a sub-diffusive manner, with significant anti-persistence, resulting in more variation in sister cells at the end of their lifetimes.

data is needed to confirm this is a robustly appropriate choice, elucidate the parameters for other experimental conditions and investigate how this is affected by cell-cell interactions. Note that this allows us to capture the nature of the variation in OCT4 only and further aspects of the behaviour need to be considered to fully describe the OCT4 regulation over time.

Although this shows that overall, positive changes in OCT4 are just as likely to occur as negative ones, it does not reveal anything about the temporal nature of these fluctuations and hence any correlation properties which may be evident over time (for example, all the positive changes in OCT4 could come one after the other, followed by all the negative changes, it doesn't mean that a positive change is necessarily followed by a negative change). There is also a difference in these fluctuations after the differentiation agent, with the addition of BMP4 provoking tighter self-regulation across all cell fates. Further experiments are needed to investigate whether this self-regulation is a collective behaviour effect.

A significant finding of this analysis is the quantification of the self-regulatory properties of OCT4 within cells. An autocorrelation analysis, along with the calculation of the Hurst exponent shows significant anti-persistence, in keeping with the regulation of PTFs (17, 21, 37). Throughout the colony growth, anti-persistence of at least five hours is seen in 86% of cells (with no significant difference between the cell fates), and on average occurs between 3 and 12 hours into a cell's lifetime. This is further illustrated by considering the behaviour of the cells in the diffusion framework, with cells across all fates showing significant sub-diffusivity. This not only illustrates that the cells are self-regulating their internal OCT4 abundance, but also provides a quantitative starting point for the mathematical modelling of OCT4 time series. This opens up techniques such as fractional Brownian motion, where a random time series with a certain Hurst exponent can be simulated, and correlated random walk theory.

The experiment in Ref. (27) has led to a rich analysis,

allowing us to establish the language through which to quantitatively compare this experiment to others. In general, this highlights the need for further temporal experimental data on OCT4 and other transcription factors. These quantitative analyses provide the basis for the identification of systematic behaviours, the comparison to future experimental data and the basis for the mathematical modelling of pluripotency.

CONCLUSION

AUTHOR CONTRIBUTIONS

See Ref. (27) for author contributions for the original experiment. L.E.W. analysed the data and prepared the figures. L.E.W., S.O.F., I.N., M.L., N.G.P. and A.S. wrote the manuscript.

ACKNOWLEDGEMENTS

IN acknowledges the grant from the Russian Government 641 Program for the recruitment of the leading scientists into 641 Russian Institution of Higher Education 14.w03.31.0029 and RFFI project GRANT number 20-015-00060.

REFERENCES

1. Ebert, A. D., and C. N. Svendsen, 2010. Human stem cells and drug screening: opportunities and challenges. *NRDD* 9:367–372.
2. Zhu, Z., and D. Huangfu, 2013. Human pluripotent stem cells: an emerging model in developmental biology. *Development* 140:705–717.
3. Avior, Y., I. Sagi, and N. Benvenisty, 2016. Pluripotent stem cells in disease modelling and drug discovery. *NRMCB* 17:170–182.

4. Ilic, D., and C. Ogilvie, 2017. Concise Review: Human Embryonic Stem Cells - What Have We Done? What Are We Doing? Where Are We Going? *Stem Cells* 35:17–25.
5. Shroff, G., J. D. Titus, and R. Shroff, 2017. A review of the emerging potential therapy for neurological disorders: human embryonic stem cell therapy. *AJSC* 6:1.
6. Trounson, A., and N. D. DeWitt, 2016. Pluripotent stem cells progressing to the clinic. *NRMCB* 17:194.
7. Bauwens, C. L., R. Peerani, S. Niebruegge, K. A. Woodhouse, E. Kumacheva, M. Husain, and P. W. Zandstra, 2008. Control of human embryonic stem cell colony and aggregate size heterogeneity influences differentiation trajectories. *Stem Cells* 26:2300–2310.
8. MacArthur, B. D., and I. R. Lemischka, 2013. Statistical mechanics of pluripotency. *Cell* 154:484 – 489.
9. Torres-Padilla, M.-E., and I. Chambers, 2014. Transcription factor heterogeneity in pluripotent stem cells: a stochastic advantage. *Development* 141:2173–2181.
10. Shuzui, E., M. Kim, and M. Kino-oka, 2019. Anomalous cell migration triggers a switch to deviation from the undifferentiated state in colonies of human induced pluripotent stems on feeder layers. *JBB* 127:246 – 255.
11. Stadhouders, R., G. J. Fillion, and T. Graf, 2019. Transcription factors and 3D genome conformation in cell-fate decisions. *Nature* 569:345–354.
12. Nemashkalo, A., A. Ruzo, I. Heemskerk, and A. Warmflash, 2017. Morphogen and community effects determine cell fates in response to BMP4 signaling in human embryonic stem cells. *Development* 144:3042–3053.
13. Rosowski, K. A., A. F. Mertz, S. Norcross, E. R. Dufresne, and V. Horsley, 2015. Edges of human embryonic stem cell colonies display distinct mechanical properties and differentiation potential. *SR* 5:14218.
14. Pauklin, S., and L. Vallier, 2013. The Cell-Cycle State of Stem Cells Determines Cell Fate Propensity. *Cell* 155:135 – 147.
15. Hwang, N. S., S. Varghese, and J. Elisseeff, 2008. Controlled differentiation of stem cells. *ADDR* 60:199 – 214. Emerging Trends in Cell-Based Therapies.
16. Warmflash, A., B. Sorre, F. Etoc, E. D. Siggia, and A. H. Brivanlou, 2014. A method to recapitulate early embryonic spatial patterning in human embryonic stem cells. *NM* 11:847–854.
17. Li, M., and J. C. Izpisua Belmonte, 2018. Deconstructing the pluripotency gene regulatory network. *NCB* 20:382–392.
18. Boyer, L. A., T. I. Lee, M. F. Cole, S. E. Johnstone, S. S. Levine, J. P. Zucker, M. G. Guenther, R. M. Kumar, H. L. Murray, R. G. Jenner, D. K. Gifford, D. A. Melton, R. Jaenisch, and R. A. Young, 2005. Core transcriptional regulatory circuitry in human embryonic stem cells. *Cell* 122:947—956.
19. Chambers, I., and S. R. Tomlinson, 2009. The transcriptional foundation of pluripotency. *Development* 136:2311–2322.
20. Kumar, R. M., P. Cahan, A. K. Shalek, R. Satija, A. DaleyKeyser, H. Li, J. Zhang, K. Pardee, D. Gennert, J. J. Trombetta, T. C. Ferrante, A. Regev, G. Q. Daley, and J. J. Collins, 2014. Deconstructing transcriptional heterogeneity in pluripotent stem cells. *Nature* 516:56–61.
21. Wang, Z., E. Oron, B. Nelson, S. Razis, and N. Ivanova, 2012. Distinct lineage specification roles for NANOG, OCT4, and SOX2 in human embryonic stem cells. *Cell Stem Cell* 10:440 – 454.
22. Symmons, O., and A. Raj, 2016. What's luck got to do with it: single Cells, multiple fates, and biological non-determinism. *MC* 62:788 – 802.
23. Singh, A. M., J. Chappell, R. Trost, L. Lin, T. Wang, J. Tang, H. Wu, S. Zhao, P. Jin, and S. Dalton, 2013. Cell-Cycle Control of Developmentally Regulated Transcription Factors Accounts for Heterogeneity in Human Pluripotent Cells. *Stem Cell Reports* 1:532 – 544.
24. Niwa, H., J. Miyazaki, and A. G. Smith, 2000. Quantitative expression of Oct-3/4 defines differentiation, dedifferentiation or self-renewal of ES cells. *NG* 24:372–376.
25. Kopp, J. L., B. D. Ormsbee, M. Desler, and A. Rizzino, 2008. Small increases in the level of Sox2 trigger the differentiation of mouse embryonic stem cells. *Stem cells* 26:903–911.
26. Streibinger, D., C. Deluz, E. T. Friman, S. Govindan, A. B. Alber, and D. M. Suter, 2019. Endogenous fluctuations of OCT4 and SOX2 bias pluripotent cell fate decisions. *MSB* 15:e9002. <https://www.embopress.org/doi/abs/10.15252/msb.20199002>.
27. Wolff, S. C., K. M. Kedziora, R. Dumitru, C. D. Dungee, T. M. Zikry, A. S. Beltran, R. A. Haggerty, J. Cheng, M. A. Redick, and J. E. Purvis, 2018. Inheritance of OCT4 predetermines fate choice in human embryonic stem cells. *Mol. Syst. Biol.* 14:e8140.
28. Skamagki, M., K. B. Wicher, A. J., S. Ganguly, and M. Zernicka-Goetz, 2013. Asymmetric Localization of Cdx2 mRNA during the First Cell-Fate Decision in Early Mouse Development. *Cell Reports* 3:442 – 457.

29. Tee, W.-W., and D. Reinberg, 2014. Chromatin features and the epigenetic regulation of pluripotency states in ESCs. *Development* 141:2376–2390.
30. Holmes, W. R., N. S. Reyes de Mochel, Q. Wang, H. Du, T. Peng, M. Chiang, O. Cinquin, K. Cho, and Q. Nie, 2017. Gene Expression Noise Enhances Robust Organization of the Early Mammalian Blastocyst. *PLoSCB* 13:1–23.
31. Wadkin, L. E., S. Orozco-Fuentes, I. Neganova, M. Lako, A. Shukurov, and N. G. Parker, 2020. The recent advances in the mathematical modelling of human pluripotent stem cells. *SN Applied Sciences* 2:276.
32. Pir, P., and N. Le Novère, 2016. Mathematical models of pluripotent stem cells: at the dawn of predictive regenerative medicine. *In Systems Medicine*, Springer, 331–350.
33. Chickarmane, V., C. Troein, U. A. Nuber, H. M. Sauro, and C. Peterson, 2006. Transcriptional Dynamics of the Embryonic Stem Cell Switch. *PLoS* 2:1–13. <https://doi.org/10.1371/journal.pcbi.0020123>.
34. Glauche, I., M. Herberg, and I. Roeder, 2010. Nanog Variability and Pluripotency Regulation of Embryonic Stem Cells - Insights from a Mathematical Model Analysis. *PLOS* 5:1–12. <https://doi.org/10.1371/journal.pone.0011238>.
35. Herberg, M., and I. Roeder, 2015. Computational modelling of embryonic stem-cell fate control. *Development* 142:2250–2260.
36. Xu, H., Y.-S. Ang, A. Sevilla, I. R. Lemischka, and A. Ma'ayan, 2014. Construction and Validation of a Regulatory Network for Pluripotency and Self-Renewal of Mouse Embryonic Stem Cells. *PLoS* 10:1–14.
37. Akberdin, I. R., N. A. Omelyanchuk, S. I. Fadeev, N. E. Leskova, E. A. Oschepkova, F. V. Kazantsev, Y. G. Matushkin, D. A. Afonnikov, and N. A. Kolchanov, 2018. Pluripotency gene network dynamics: System views from parametric analysis. *PLOS* 13:1–24.
38. Auddya, D., and B. J. Roth, 2017. A mathematical description of a growing cell colony based on the mechanical bidomain model. *JPhysD* 50:105401.
39. Babaie, Y., R. Herwig, B. Greber, T. C. Brink, W. Wruck, D. Groth, H. Lehrach, T. Burdon, and J. Adjaye, 2007. Analysis of Oct4-dependent transcriptional networks regulating self-renewal and pluripotency in human embryonic stem cells. *Stem cells* 25:500–510.
40. Ghule, P. N., R. Medina, C. J. Lengner, M. Mandeville, M. Qiao, Z. Dominski, J. B. Lian, J. L. Stein, A. J. van Wijnen, and G. S. Stein, 2011. Reprogramming the pluripotent cell cycle: Restoration of an abbreviated G1 phase in human induced pluripotent stem (iPS) cells. *JCP* 226:1149–1156.
41. Wadkin, L. E., S. Orozco-Fuentes, I. Neganova, S. Bojic, A. Laude, M. Lako, N. G. Parker, and A. Shukurov, 2019. Seeding hESCs to achieve optimal colony clonality. *SR* 9:15299.
42. Panyutin, I. V., S. A. Holar, R. D. Neumann, and I. G. Panyutin, 2017. Effect of ionizing radiation on the proliferation of human embryonic stem cells. *SR* 7:43995.
43. Mandelbrot, B. B., and J. W. Van Ness, 1968. Fractional Brownian motions, fractional noises and applications. *SIAM Rev* 10:422–437.
44. Mielniczuk, J., and P. Wojdyło, 2007. Estimation of Hurst exponent revisited. *Comput. Stat. Data Anal* 51:4510–4525.
45. Lacasa, L., B. Luque, J. Luque, and J. C. Nuno, 2009. The visibility graph: A new method for estimating the Hurst exponent of fractional Brownian motion. *EPL* 86:30001.
46. Barunik, J., and L. Kristoufek, 2010. On Hurst exponent estimation under heavy-tailed distributions. *PHYSICA A* 389:3844–3855.
47. Sveshnikov, A. A., I. N. Sneddon, and M. Stark, 1966. *Applied Methods of the Theory of Random Functions*. ISSN. Elsevier Science.
48. Murray, J. D., 2002. *Mathematical Biology I. An Introduction*, volume 17 of *Interdisciplinary Applied Mathematics*. Springer, New York, 3 edition.
49. Codling, E. A., M. J. Plank, and S. Benhamou, 2008. Random walk models in biology. *J. R. Soc. Interface* 6:813–834.
50. Zaret, K. S., 2014. Genome reactivation after the silence in mitosis: recapitulating mechanisms of development? *DC* 29:132–134.
51. Festuccia, N., I. Gonzalez, N. Owens, and P. Navarro, 2017. Mitotic bookmarking in development and stem cells. *Development* 144:3633–3645.
52. Li, L., B. H. Wang, S. Wang, L. Moalim-Nour, K. Mohib, D. Lohnes, and L. Wang, 2010. Individual cell movement, asymmetric colony expansion, rho-associated kinase, and E-cadherin impact the clonogenicity of human embryonic stem cells. *Biophys.* 98:2442 – 2451.
53. Wu, P., A. Giri, S. X. Sun, and D. Wirtz, 2014. Three-dimensional cell migration does not follow a random walk. *Proc. Natl. Acad. Sci. U.S.A.* 111:3949–3954.

54. Wadkin, L. E., L. F. Elliot, I. Neganova, N. G. Parker, V. Chichagova, G. Swan, A. Laude, M. Lako, and A. Shukurov, 2017. Dynamics of single human embryonic stem cells and their pairs: a quantitative analysis. *SR* 7:1–12.
55. Wadkin, L. E., S. Orozco-Fuentes, I. Neganova, G. Swan, A. Laude, M. Lako, A. Shukurov, and N. G. Parker, 2018. Correlated random walks of human embryonic stem cells in vitro. *IOP Phys. Biol.* 15:056006.

SUPPLEMENTARY MATERIAL

An online supplement to this article can be found by visiting BJ Online at <http://www.biophysj.org>.